TEST PROGRAM TO DEVELOP AND EXTEND TECHNOLOGICAL MATURITY OF A WEIGHT-OPTIMIZED SINGLE-PIECE COMPOSITE DRIVE SHAFT FOR TAIL DRIVE LINE APPLICATION

Sébastien BARLET-BAS, Research & Innovation engineer, Nexteam Group, Launaguet, France
François MALBURET, Associate Professor, Arts et Métiers – LISPEN lab., Aix-en-Provence, France
Cédric LOPEZ, Engineering & Innovation Director, Nexteam Group, Marignane, France
Bruno PIERREL, Research & Innovation Manager, Nexteam Group, Launaguet, France
Axel MORICAUD, Project Engineer, Nexteam Group, Marignane, France
Bassem, BEN SAÏD, Research Engineer, Arts et Métiers – LISPEN lab., Aix-en-Provence, France

Abstract

The submitted paper aims to present the test campaign implemented to assess the development of a single-piece composite drive shaft. This part is a component of a mechanical drive line using innovative composite drive shafts with integrated composite flanges for tail drive line helicopter. This work is part of the RECOMPOSE (aRbrE COMPOSitE) project funded by the European Union NextGeneration EU, the DGAC (French Civil Aviation Authority) and supported by CORAC (Civil Aviation Research Council), from July 2021 to July 2025, and with Airbus Helicopters as sponsor. The overall goal aims to increase the competitiveness of helicopters while reducing their CO2 emissions, and the project team was made up of Nexteam group (tier 1 aerospace and defense supplier and manufacturer – France), CT Ingénierie (innovation and engineering services - France) and Arts et Métiers through their research valorization department AMVALOR (University - France). The tests performed have been useful to gain knowledge about the mechanical and dynamical behavior of the composite shaft and enlighten about the strength of the composite flange.[1]

1. INTRODUCTION AND PROBLEMATIC

The development of lightweight and high-performance components is a key challenge in modern helicopter design. This paper presents the testing of a single-piece composite drive shaft, aiming to highly decrease the number of operations to manufacture and assemble conventional metallic flanges with composite tubes (Ref. 1, 2) thanks to a simplified and innovative manufacturing process. The use of composite materials offers significant mass savings, reducing overall helicopter weight and improving fuel efficiency. As explained in (Ref. 3), such a composite drive shaft helps to extend mass savings by increasing the bending critical frequencies of the transmission line at their limits thanks to high modulus properties of the carbon fiber. This implies that drive shafts can be longer than metallic ones, thus the number of other components like supports and bearings could be reduced, helping to save additional weight. The single-piece composite definition is innovative in many aspects. Firstly, the design of this kind of part is not determined by standard since composite final properties are highly linked to the newly developed manufacturing process used to build the part (Ref. 3). This work has simultaneously focused on design methods and manufacturing processes to improve the maturity level of this part, and presents the tests performed to validate this couple design-manufacturing processes. Secondly, the manufacturing process to obtain this kind of monolithic flange is complex to execute to master the fiber positioning but provides new kind of parts with improved mass and mechanical properties (Ref. 3) compared to metallic ones.

In literature, or in design method, various aspects are considered to size and develop drive shaft. Firstly, these parts have to transmit torque and many papers discuss the torsional strength of the tubular section (Ref. 4, 5). In this case, the torsional strength of the composite flange needs to be assessed too and no work has currently explored this subject since it is related to a new manufacturing process. This first limitation about sizing method is not the point of this paper, but experimental data points are needed to construct this method and correlate engineering models, and this is what this work is focused on. To perform this task, failure of fully composite flanges in torsion data is collected by multiple torsional failure of composite drive shafts.

Composite materials exhibit fatigue behavior that differs significantly from that of traditional metals, primarily due to their heterogeneous and anisotropic nature. Composites generally have higher fatigue threshold stresses than metals, but with higher variability once this level is exceeded (Ref. 11). In metals, fatigue typically involves the initiation and propagation of cracks under cyclic loading. In contrast, composites experience a range of damage mechanisms such as matrix cracking, fiber-matrix debonding, delamination, and fiber breakage (Ref. 6). Instead, composites may accumulate damage over time even at low stress levels, leading to progressive deterioration in mechanical properties (Ref. 7). The anisotropic nature of composites means that fatigue performance is highly dependent on the orientation of fibers relative to the applied load, necessitating careful design considerations to optimize fatigue resistance. Because of the complex fiber orientation and the diversity of load cases in the composite flange, the expected lifecycle cannot be predicted based on a single material fatigue curve. Therefore, various fatigue tests are performed on the composite drive shaft, to build a fatigue curve specific to the composite flange and its manufacturing process. Theoretical models to predict fatigue failure could then be developed based on these experimental results.

As explained in (Ref. 8), composite drive shafts could be subject to whirl instabilities in operations because of the internal (or rotating) damping of the composite material. This is likely to appear for supercritical shafts, meaning they cross one or several critical frequencies in bending. Even if the main architecture developed on the RECOMPOSE project use case is subcritical, other supercritical configurations have also been studied and that is why dynamic tests are performed. The dynamic behavior of the single-piece composite drive shaft is studied near its first critical frequency, but not crossed, to confirm the healthy dynamic of the shaft. Internal damping in composites arises from mechanisms like matrix viscoelasticity and fiber-matrix interactions. While damping typically dissipates vibrational energy, in rotating systems, it can introduce destabilizing forces, especially beyond certain rotational speeds (Ref. 9, 10). To be sure to master all the design of the shaft, dynamic tests are implemented to ensure the lack of instabilities in realistic test conditions, as close as possible as the transmission driveline in operation. This includes representative parts like support or flexible couplings, but also the impact analysis of axial and angular misalignments.

2. THE SINGLE-PIECE COMPOSITE DRIVE SHAFT

As previously explained, the innovative part of this composite drive shaft is the flange and its connection to the tube which is made in the same phase and with the same material as the one used within the tubular section (Ref. 3). The RECOMPOSE project defined a list of specifications that the shaft needs to satisfy, and the shafts have been designed upon it. Several prototypes have been manufactured according to the same process in order to ensure the following points. Firstly, that the manufacturing process is repeatable enough according to aeronautical standards. Secondly, to assess the mechanical, dynamical or any other behavior of the shaft with experimental tests, to confirm compliance with specifications. Various shortened prototypes had been previously manufactured and tested to develop and improve the design and manufacturing processes. An example of the manufactured prototypes is presented in Figure 1. In addition, a balancing ring made of steel material is integrated (comoulded during polymerization step) at each side of the shaft to help balance the shaft in rotation. One or more additional ring can be added along the shaft as friction (and balancing if need) bush to guide the dynamical behavior of the composite shaft, mostly in supercritical modes.

The following sections introduce the test facilities and the test programs used to investigate the capabilities and the limits of these composite drive shafts.

Figure 1: Picture of the tube flange connection of a RECOMPOSE single-piece composite drive shaft

3. TEST FACILITIES AND INSTRUMENTATION

The test campaign was conducted using two dedicated test benches, each designed for a specific aspect of the composite drive shaft evaluation.

The first test bench is focused on dynamic analysis, utilizing an electric motor capable of rotating a drive line up to 6 meters long at a speed of 120 Hz, see Figure 2. This test bench has been developed by and for ENSAM/AMVALOR research activities. Shaft deflection is measured with laser displacement sensors (in Y and Z axis if X-axis is along the shaft), while supports vibrations are measured thanks to accelerometers along both Y and Z axis. The shafts are not instrumented for these tests, but telemetry data is conceivable if stress values are needed. Dynamic tests enable to check about the balancing quality of the shaft, the dynamic behavior regarding various speed levels and their stability at subcritical range firstly. These tests also help to assess the behavior under misalignment and its impact on the vibration level and the stability. Five configurations are studied in the project, according to the Figure 4, with the first two studying a shaft alone with different kinds of supports. The three others configuration study a reduced drive line made of two RECOMPOSE drive shafts and various kinds of supports. Each shaft end is connected to a support through a flexible coupling designed to recover angular misalignment.

The second test bench has been designed for low-cycle fatigue testing by ENSAM/AMVALOR and NEXTEAM, and is situated in ENSAM facilities, see Figure 3. The torque is applied through a hydraulic actuator that applied cyclic loading on a lever arm mechanism. This system enabled the application of high torques, depending on the lever arm length and the hydraulic actuator force, allowing for controlled fatigue cycling at determined torque amplitudes.

Figure 2: Test bench used for dynamic tests

This test bench provided essential data on the fatigue life of the composite drive shaft under various loading in torsion (with or without misalignment), helping to refine durability predictions and ensure structural reliability. Data acquisition is achieved by the mean of a force sensor in the hydraulic actuator (giving the torque applied once the lever arm and the angle of the force are considered), an angle sensor to get the torsion angle of the shaft and a torquemeter to get a “true” value of the torque applied on the shaft. Other sensors are installed on the shaft itself like strain gauges. Three strain rosettes are placed along the shaft: one at 1/3 of the length and another at 2/3 of the length to measure torsional stresses. The third sensor is positioned near the connecting radius of the flange to evaluate stress concentrations in this critical area. In addition to these rosettes, unidirectional strain gauges are installed at the 1/3 and 2/3 length positions to specifically measure shaft deflection under torsional loading. Given the complexity of stress distribution around the flange because of the mix of stress concentrations (holes, radius), different positions of rosettes are considered depending on the position compared to the fixation holes : 15° before and after the non-fixation hole, and 15° before and after fixation holes. This comprehensive instrumentation strategy ensured precise monitoring of the drive shaft’s mechanical behavior, enabling validation of numerical models and optimization of the composite design.

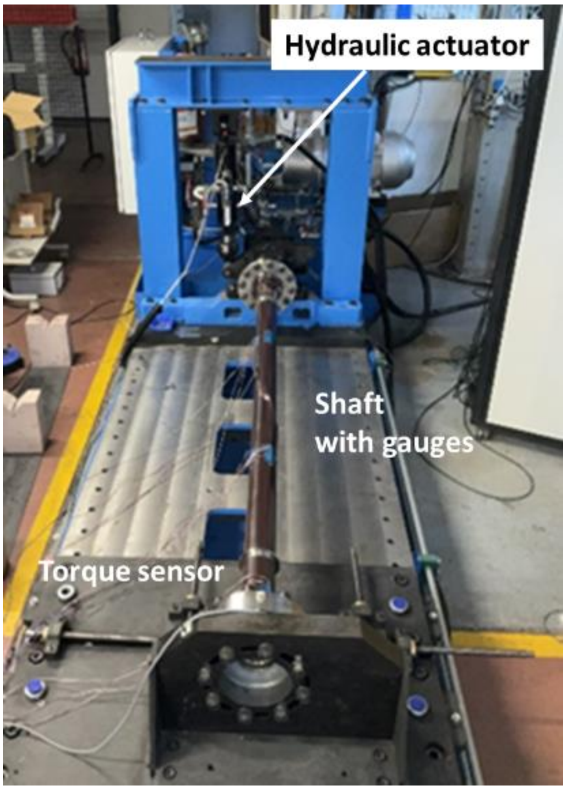

Figure 3: Test bench used for torsional static and low fatigue tests

4. TEST PROGRAM

4.1. Torsional stiffness characterization

Torsional characterization tests are conducted to measure the global stiffness of drive shafts, including both the flanges and the tube, mounted on two flexible couplings (flectors). The primary objective of these tests is twofold: first, to ensure repeatability of the stiffness values across different shafts, which serves as an indicator of consistent manufacturing quality; and second, to validate that the experimental values are in agreement with those predicted by numerical models. Stiffnesses measured during these tests include the combination of stiffness of the shaft and two flectors in series. The global stiffness measured is then composed of :

$$\frac{1}{K_{eq}} = \frac{1}{K_{shaft}} + \frac{2}{K_{flector}} \quad (1)$$

The stiffness of the shaft alone is measured in the static failure test and in fatigue tests because flectors cannot withstand such high torque levels. The combination of the global stiffness $\mathrm{K_{eq}}$ and the shaft stiffness $\mathrm{K_{shaft}}$ serves to determine the flector stiffness $\mathrm{K_{flector}}$.

To achieve this global stiffness characterization, a batch of ten shafts was subjected to torsional loading using the torsional fatigue testing bench (LCF). The loading sequence involves multiple phases of torque increase and decrease, as illustrated in the left column of Figure 5. The torque profile begins with a gradual ramp-up to 800 Nm, followed by a partial unloading to 200 Nm to maintain tension and account for potential clearance settling. A second ramp-up is then applied, returning the torque to 800 Nm, and finally increasing to 1200 Nm before fully unloading the shaft. At each loading set, the torque is held for a minimum of three seconds to stabilize the measurement and comply with load validation protocols, in line with certification requirements such as those outlined in CS-29—even though the applied torques during these tests remain below ultimate load specifications.

Stiffness is computed through regression analysis of the torque versus angle curves, by computing the slope of the curve and the determination coefficient R^2 associated. Several stiffness values are extracted from distinct sections of the loading path, specifically in the intervals: [0–800], [800–200], [200–800], [800–1200], and [1200–0] Nm.

Each test is repeated three times per shaft to ensure proper clearance setting and to assess the variability of the measurements. Additionally, two accelerometers are mounted on the tube near each flange to detect abnormal noises or vibrations, such as fiber breakage events, which may manifest as audible snapping sounds.

4.2. Shaft failure in torsion

Two shafts were tested to failure under static torsional loading: a short prototype shaft and a RECOMPOSE shaft. The aim of these tests was to determine the maximum torsional load that the newly designed composite flange can withstand, and how the failure occurs to determine the weaker part of the flange or tube. As previously explained, the flexible couplings are removed for these tests to prevent a failure of these components before the shaft.

The applied torque profile followed the same kind of methodology as the stiffness characterization tests. Initially, the torque was increased from 0 to 1200 Nm to ensure proper clearance settlement. This was followed by a partial unloading to 400 Nm, then a progressive increase in torque until failure occurred. The torque was incremented in gradual steps, ranging from several tens to a few hundred Newton-meters, with each plateau maintained for at least three seconds to ensure measurement stability and the strength of the shaft under extended loading.

The same set of measurements was recorded as during the stiffness characterization tests: applied torque, shaft torsion angle, and accelerometer signals for detecting abnormal noises such as fiber breakage. In addition, strain gauges were used to measure local deformations on the tube as well as near the flange, particularly at the transition zone close to the fillet radius.

4.3. Fatigue characterization

The purpose of these tests is to directly obtain the actual torsional fatigue curve of the newly developed monolithic composite shaft. This experimental campaign builds on the prior static failure tests, as the rupture torque values derived from those tests provide the starting points of the fatigue curve—namely, the fatigue limit corresponding to a very low number of cycles. The instrumentation used for data acquisition is identical to that employed during the stiffness and static torsional failure tests, including torque and angular displacement sensors, accelerometers, and strain gauges.

Since the fatigue curve is not known a priori, neither is the torque amplitude required to achieve a specific theoretical number of cycles. Therefore, the testing strategy becomes an iterative process aimed at systematically determining the torque amplitudes necessary to construct the fatigue curve. The first test point is typically selected as a percentage of the previously determined static rupture torque, for instance 80% or 90%. Another key consideration when defining the applied torque amplitude is the desired type of fatigue curve. In the case of a helicopter tail rotor driveshaft, the torque rarely drops to zero during operation, and no load reversal occurs. As such, the targeted fatigue curve is of type $R = 0.1$, meaning the load cycles between a high value and a non-zero minimum (typically around 10% of the maximum torque).

Once the first point is established, an initial estimation of the curve can be made using a standard fatigue law for composites, such as Basquin's or Weibull's model. Subsequent torque amplitudes are then selected either graphically or through predictive use of the chosen fatigue law. Repeating this process progressively populates the curve and increases confidence in the experimentally derived fatigue behavior.

The test stop condition is a crucial aspect of the methodology. According to CS-29 certification guidelines, several fatigue limit criteria can be considered, especially for components with known defects:

- No Growth: the test is stopped as soon as defect propagation is observed.
- Slow Growth: propagation is permitted only if it is slow, controlled, and predictable.
- Arrested Growth: defect growth is allowed but must be mechanically halted before reaching a critical size.

In the case of defect-free shafts, these criteria do not apply. Instead, two criteria are used to terminate the fatigue test:

- A stiffness reduction exceeding a specified percentage of the initial average stiffness.
- Visible damage to the shaft (e.g., cracks, delamination).

4.4. Dynamic characterization

The majority of industrial rotating shafts, and particularly aeronautics, operate in subcritical conditions to avoid crossing resonance modes during ramp-ups. The subcritical domain is widely present in practice, and well documented in the classical literature on rotor dynamics. For metal shafts, subcritical behavior has been modeled for a long time, with robust results. Imbalance, misalignment, stiffness, bending modes are well integrated into linear models. In the case of composite shafts, the dynamic behavior is a direct result of the architecture of the laminate, the fiber and the materials used. These characteristics significantly influence dynamic behavior.

The first part of this experimental phase aims to characterize experimentally the vibration behavior of the proposed configuration, using dynamic tests to precisely identify the location of the modes and the associated damping levels.

A second part of the tests integrates the representative elements of a complete shaft line, taking into account the couplings (flector) as well as the bearings. The aim is to reproduce the real installation conditions as well as possible in order to assess the influence of the overall architecture on the dynamic behavior. In particular, these tests make it possible to identify possible couplings between sections as well as effects related to mechanical interfaces (flexible connections, clearances or localized damping). This approach aims to go beyond the simple modal characterization of the shaft alone, to take into account the dynamic phenomena induced by the integration of the component in a complex transmission chain.

In order to accurately characterize the dynamic behavior in the subcritical regime, a test protocol structured in several steps has been defined. This step-by-step approach aims to isolate and then combine the key mechanical effects involved in the vibrational behavior of the system. The objective of the protocol is threefold:

- Identify the natural frequencies and dominant modes of the structure,
- Characterize the overall damping under different mounting conditions,
- Analyze the influence of mechanical variables such as interfaces (flectors, bearings), misalignments and coupling between sections.

In the case of composite shafts, the dynamic behavior cannot be reduced to that of an isotropic shaft: it depends on the stratified, the mass distribution, the bonds, and the mechanical interfaces. In addition, the vibrational amplitudes in the subcritical regime are low, which makes the phenomena sensitive to the experimental environment. The protocol put in place aims to distinguish between intrinsic effects (related to the structure itself) and extrinsic effects (due to the assembly or associated components). It is also a question of testing the robustness of modal behavior under conditions close to real use.

The protocol followed consists of three phases:

(a) Non-rotational modal testing. Composite shaft alone, in free-free conditions with shock hammer excitation and measurement of the vibration response by accelerometers. The objective is to establish a reference modal signature, without the influence of interfaces or rotational motion.

(b) Dynamic tests with a single section (in rotation). The shaft is mounted on the bench with flectors and bearings. Two versions of bearings were available: RECOMPOSE bearings with a design close to a series definition and reference "tooling" bearings (ENSAM bearing) of the bench. The procedure consists of making run-up with climbs and descents, and with constant speeds for a few seconds. There is the technical possibility of introducing controlled misalignments. The objective is to observe the changes in modal behavior, the evolution of damping, and the sensitivity to misalignment during transient phases and regimes at stabilized speeds.

(c) Dynamic tests with two sections (in rotation). The tested configurations consist of two sections in series with an intermediate bearing between the sections. The test procedure is the same as for the tap tests and the run-up and speed stabilization phases. The objective is to analyze the effects of dynamic coupling between sections, and the distribution of eigenmodes throughout the line.

This progressive experimental approach makes it possible to document the impact of each component (shaft, flector, bearing) and each assembly parameter on the overall vibration behavior, while building a solid basis for a recalibration of knowledge models (Figure 11 and 12).

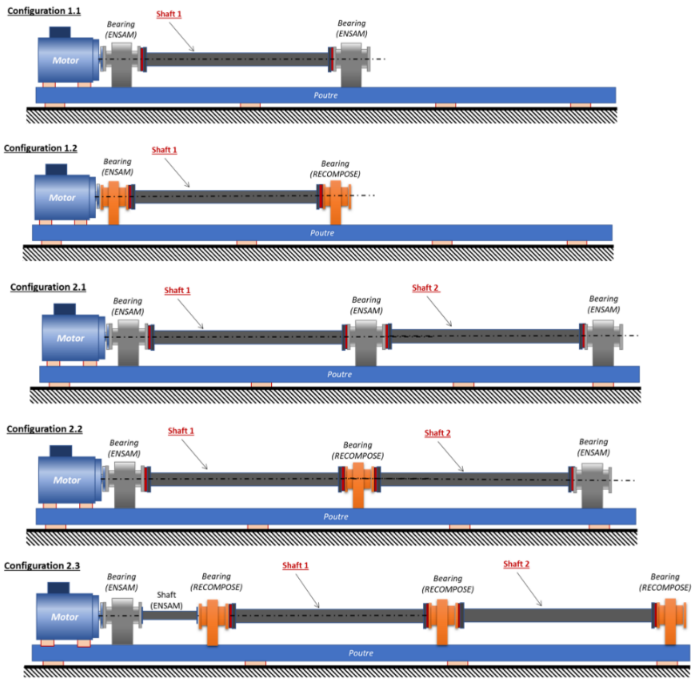

Figure 4:Various configurations tested for dynamic characterization

5. EXPERIMENTAL RESULTS

5.1. Torsional stiffness characterization

As a reminder, each stiffness characterization test has been repeated three times in order to observe the settling of mechanical clearances during assembly and to assess the repeatability of the measured data. All experimental results were plotted individually for each shaft, as shown in Figure 5 for the reference shaft 006 (and two flexible couplings).

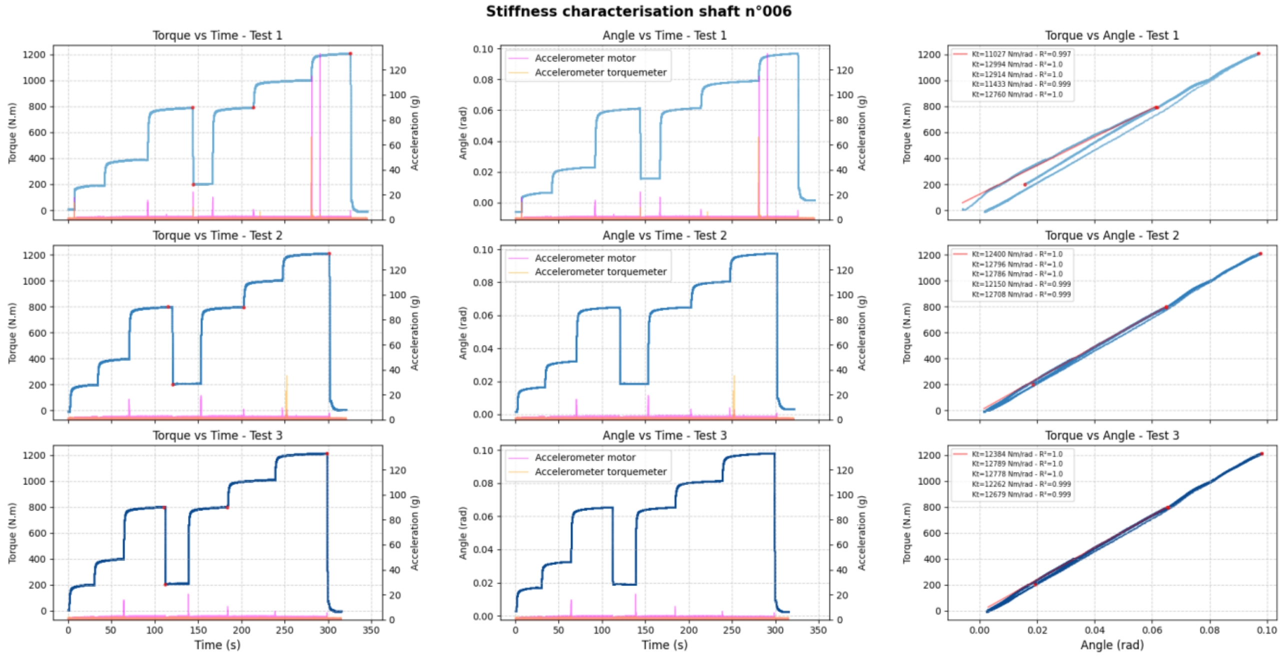

Figure 5:Stiffness characterization data on the shaft 006

The plotted data for shaft 006 demonstrates that both the torque and angular displacement profiles conform well to the expected instructions. It is important to note that the global load profile is not automated or servo-controlled—it is manually applied. Regarding the accelerometer signals, small peaks are observed at the onset of each new torque ramp. These are attributed to mechanical noise generated by the startup of the hydraulic actuator. However, two distinct peaks—likely indicative of fiber breakage—were recorded during the final ramp-up to 1200 Nm in the first test. These anomalies do not reappear in the subsequent two tests, suggesting that the internal stresses within the composite structure have reached equilibrium and no further overloading occurs.

In terms of stiffness behavior, the first test clearly shows the effect of assembly clearance settling. Its torque-angle curve exhibits a mismatch between the start and end points, whereas the two following tests are perfectly linear and consistent. Consequently, stiffness measurements from the first test should not be used as a reference for accurate stiffness estimation. For instance, stiffness in the first loading interval (0 to 800 Nm) increases from 11027 Nm/rad (R^2 = 0.997) in the first test to 12384 Nm/rad (R^2 = 1.0) in the second test—an increase of +12.3%. Similarly, in the fourth interval (800 to 1200 Nm), stiffness rises from 11433 Nm/rad (R^2 = 0.999) to 12262 Nm/rad (R^2 = 0.999), a gain of +7.3%. The third test provides the most representative estimation of the shaft's torsional stiffness, averaging around 12300 Nm/rad with consistent linear behavior.

A hysteresis effect, characteristic of composite materials, is also observed during partial unloading. This is particularly evident in the first test due to the initial clearances. The unloading phase (interval 2) shows a stiffness of 12994 Nm/rad, differing significantly from the initial loading phase (11027 Nm/rad). Interestingly, the subsequent reloading (interval 3) follows the path of the unloading phase, with a similar stiffness value of 12914 Nm/rad. This hysteresis behavior is also present, although to a lesser extent, in the second and third tests.

This methodology was repeated for each available shaft, yielding a statistical dataset of 15 stiffness measurements per shaft—derived from 3 tests, each segmented into 5 torque intervals. Using Python's Seaborn library, the distribution of these data were visualized with boxplots (Figure 6), where each box represents the interquartile range (IQR), the inner line denotes the median, and the whiskers capture the full range of measured values.

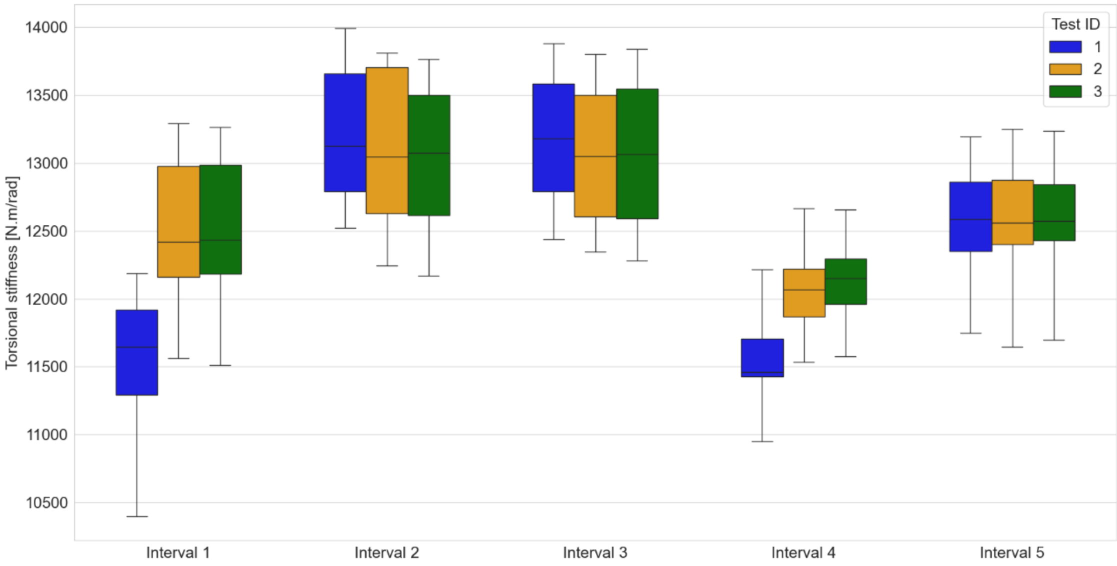

Figure 6: Stiffness distribution for each test interval of each shaft

The most relevant data for determining the true torsional stiffness of the assembly come from intervals 1 and 4. Due to the hysteresis phenomenon, stiffness values measured during intervals 2, 3, and 5 do not reflect the true mechanical behavior of the shaft under monotonic loading. Focusing on intervals 1 and 4, it is visible that stiffness from the first test (blue) is consistently lower than in subsequent tests, which continue to show slight growth. Notably, the fourth interval shows slightly lower stiffness values and reduced variance compared to the first interval during the third test: values range from 12250 to 13000 Nm/rad for the first interval (0–800 Nm), and from 12000 to 12250 Nm/rad for the fourth interval (800–1200 Nm).

The same protocol has been operated on the prototype shafts (still with two flexible couplings), including reference 013, and giving an average stiffness value of 27500 Nm/rad.

5.2. Fatigue curve

Shaft 009 (RECOMPOSE) and shaft 013 (prototype) were tested to determine the static failure torque. The test setup is identical to the static failure procedure. Two attempts were made for each shaft to position the assembly sets.

In the case of shaft 009, the first load cycle reached 1.27 times the ultimate load (ULT) without causing failure. During this first attempt, the stiffness of the shaft alone was measured at 14432 Nm/rad (R^2 = 1.0) in the range of increasing loading (because decreasing loading path follows another stiffness pattern because of hysteresis effect). The second loading reached failure at 1.82 × ULT, with a stiffness of 14482 Nm/rad (R^2 = 1.0). Acceleration readings from sensors increased by several orders of magnitude—from standard values under a few hundred g to over 10^4 g at the moment of failure. The failure event itself was abrupt, with no prior stiffness reduction and a distinct audible crack, which is consistent with expectations for a high-modulus composite material, thus with a fragile mechanical behavior.

Shaft 013, a shortened prototype with similar flanges, was also tested under static torsion to verify consistency of results. The first loading cycle reached 1.25 × ULT before being unloaded. Failure occurred during the second cycle at 1.79 × ULT, a value closely matching that of the longer shaft 009. The accelerometer signals were of the same magnitude as those from shaft 009. The torsional stiffness was calculated along the ascending loading of each attempt: 44343 Nm/rad (R^2 = 0.999) and 42291 Nm/rad (R^2 = 0.999), respectively. The increase in stiffness between the prototype shaft and RECOMPOSE shaft correlates well with the inverse of their lengths, within reasonable margin considering slight differences and uncertainties (e.g., absence of balancing rings).

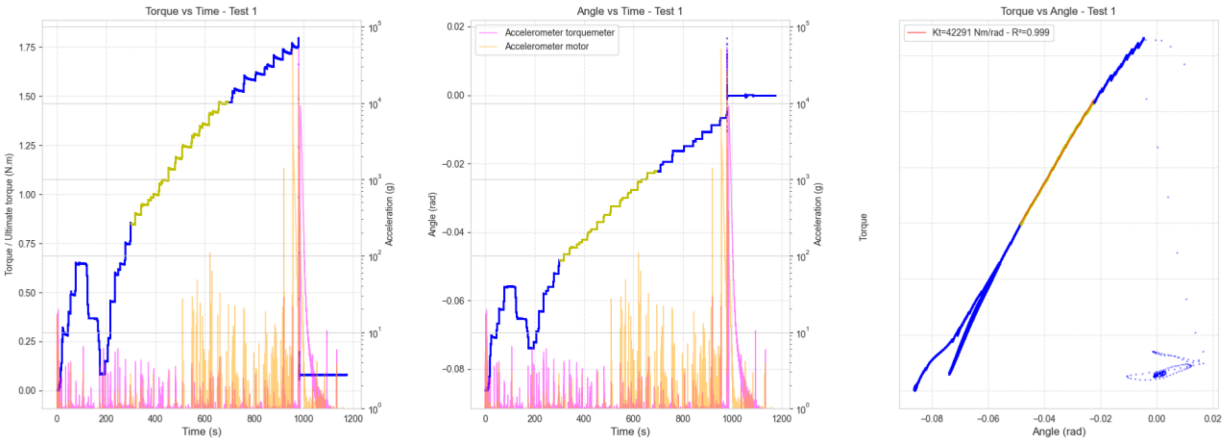

Figure 7: Data collected on failure attempt on prototype shaft 013 – torque vs time, angle vs time and torque vs angle

The two shafts failure in static present a similar failure profile. The crack seems to initiate at one of the fixation holes because of the lateral contact force applied by the screw. This crack or defect propagates quickly along the shaft up to the other flange for the shaft 013 (because of its shortened length), and up to very close of the flange (~50 mm) in the case of the shaft 009.

Figure 8: Failure of the shaft 009 in static loading

The two failure points serve as the initial data for the fatigue curve. The next step involves running R = 0.1 fatigue cycles on the shafts and recording the number of cycles to failure (or to a predefined stopping criterion). For each fatigue-tested shaft, data is post-processed using a custom Python script to visualize:

- Torque and angular displacement versus time curves,
- Analysis of peak and valley points per torque cycle, including stiffness estimation and associated R^2 value — see Figure 9
- Accelerometer signals near the actuator-side and torque transducer-side flanges.

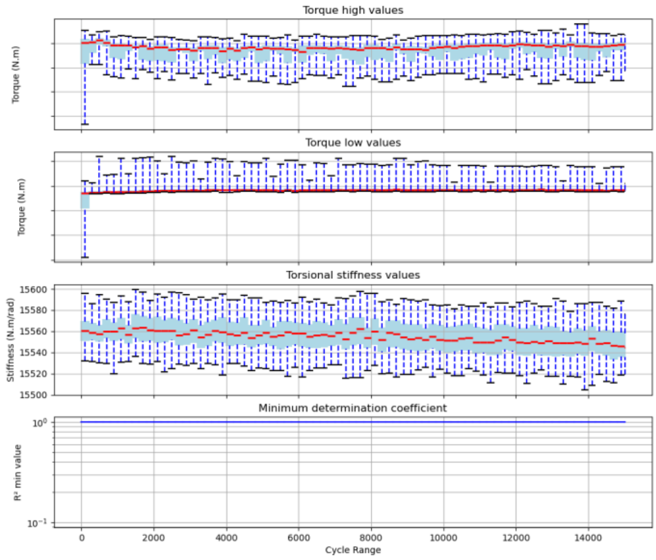

Figure 9: Example of data collected during fatigue test campaign on the shaft 005 from 65 000 cycles to 80 000 cycles (1 – torque high values distributions / 2 – torque low values distributions / 3 – torsional stiffnesses distributions / 4 – minimum of the distribution's determination coefficient)

To build the fatigue curve for the composite shaft, the following tests were conducted:

Shaft reference	Normalized dynamic torque	Dynamic / Static ratio	Number of cycles
009	1.82	1.00	1
013	1.79	1.00	1
006	1.14	0.83	200 000
003	1.39	0.84	54 518
007	1.39	0.85	570
006	1.33	0.84	119 000
012	1.38	0.85	25 083
005	1.27	0.85	253 000
008	1.47	0.85	1 495

Table 1: Summary of shafts used in torsional fatigue test

Shaft 006 was tested twice with different torque levels since it was the first shaft used in fatigue following static rupture tests. At a normalized dynamic torque of 1.14, the applied load was found too low to induce damage. According to the estimated fatigue curve in Figure 9, the ratio between completed cycles (200k) and theoretical life (29 million for the blue curve, 2.2 billion for the magenta curve) indicates negligible damage (0.7% or 0%). The shaft was then retested at a normalized dynamic torque of 1.33, reaching failure at 119k cycles.

All the failure in fatigue occurred in the same way as the failure in static : the crack initiates at a fixation hole because of the contact force of the bolt assembly. The crack propagates very quickly (because of the fragile mechanical properties) along the shaft up to the other side and stop between the two thirds of the length and the flange. The only shaft stopped before complete failure is the 005. Because a major crack sound appears during the last cycle batch, the test has been paused to investigate the material structural health, and delamination in the flange and the connecting radius seems to have happened.

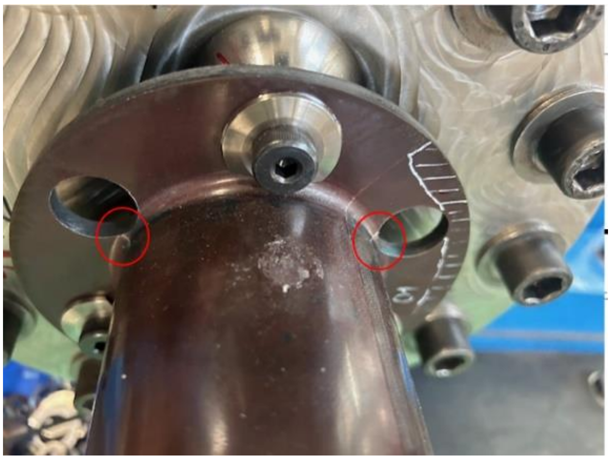

Figure 10: Failure of the surface ply in the connecting radius facing the non-fixation holes

The multiples tests in fatigue, with the same shafts that were used to measure the torsional stiffness (with flexible couplings), allow to collect data about torsional stiffness of the shafts only. The average stiffness of the RECOMPOSE and the short shaft are concatenated in the Table 2 below. Moreover, thanks to the equation (1), the stiffness can be decomposed between the RECOMPOSE shaft, the prototype shaft and the flexible couplings. The stiffness of the flexible coupling, estimated by two distinct assembly, gives similar results.

Component(s)	Stiffness value (Nm/rad)
RECOMPOSE shaft and 2 flectors	12 250
Prototype shaft and 2 flectors	27 500
RECOMPOSE shaft	14 480
Prototype shaft	42 290
Flector (RECOMPOSE assembly)	159 085
Flector (prototype assembly)	157 265

Table 2: Summary of measured stiffnesses

The fatigue behavior of the composite shaft is modeled using the Basquin law, which is well-suited for composite materials as it does not feature a classical fatigue limit (i.e., no horizontal asymptote). Instead, the fatigue limit is typically defined at 10^9 cycles. The parameter γ in the Basquin model (where formula is presented below) is material- and boundary-condition-dependent, particularly for metallic materials.

$$S = \frac{A}{N^{\gamma}} \qquad (2)$$

Two regression curves are proposed based on the defined fatigue formulation. The first (blue) includes both static and fatigue failure points, while the second (magenta) only considers fatigue failures. This distinction helps to identify potential slope variations between the low-cycle and high-cycle fatigue domains. Other fatigue curves (not presented here) have been fitted without the data point 007 which seems to have failed prematurely and without any explanation. Because it is not clear if this experimental point should be considered as an outlier or not, several fatigue curves have been tested to compare the results, and it appears that blue and magenta curves almost overlap and have the same properties with minor differences.

Analyzing the spread of data around the regression curve is crucial to refine the design criteria for composite shafts. Two distributions are typically employed to assess scatter around a mean fatigue curve: Weibull and log-normal. A Shapiro–Wilk test was applied to evaluate the normality of residuals, yielding a p-value of 0.0204. As this value is below 0.05, the distribution does not appear log-normal, and a Weibull distribution is preferred. A 95% confidence interval is plotted for each curve (with and without static points), including the impact of the possibly anomalous failure of shaft 007 as highlighted in Figure 10.

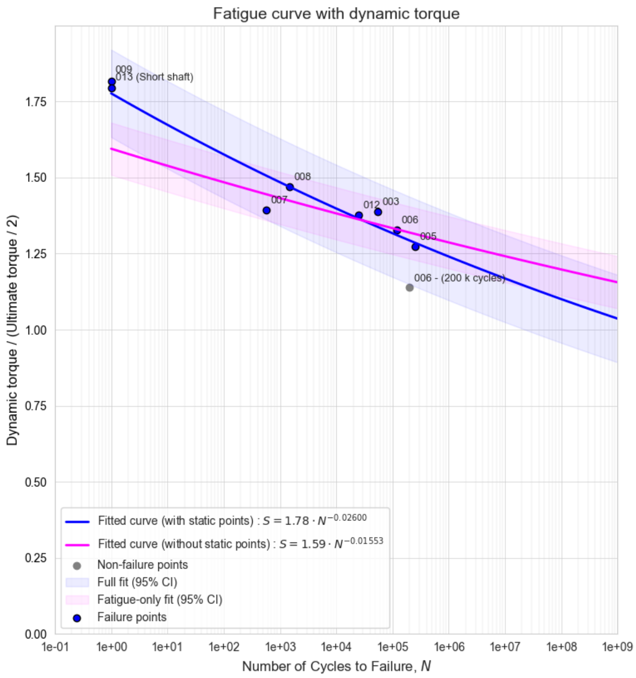

Figure 11: Regressions of fatigue curves based on data points collected during RECOMPOSE test campaign with static failure points (in blue) and without (in magenta)

5.3. Stiffness correlation with numerical model

A finite element model of the composite driveshaft was developed to compare and correlate the numerically predicted torsional stiffness with the values measured experimentally. The model was constructed using Patran and solved using Nastran. It employs 2D shell elements (CQUAD4 and CTRIA3) located at the mid-surface of the thickness from the one side to the other one: the flange, the transition radius, and the tube. Element size is refined to 1 mm in the flange region and 4 mm in the tube, with a gradual mesh transition between these zones. The model accurately represents the geometry of the various components—tube, balancing rings, flanges, and titanium attachment rings—as well as the material properties. For instance, the titanium fixation rings are modelled explicitly around the bolt holes, as represented in the Figure 12.

The applied torque is introduced via a rigid RBE3 element connected to the nodes surrounding the bolt holes on one flange. The nodes on the opposite flange's bolt circle are fully constrained to prevent any displacement, simulating fixed boundary conditions.

When a torque of 1200 Nm is applied, the model predicts an angular rotation of 0.08881 radians. This yields a computed torsional stiffness of 13512 Nm/rad for the entire composite shaft. Compared to the values from the Table 2 the numerical model returns a stiffness 6.7 % lower than what is measured by experiments, which is a conservative result. It is interesting to note that the stiffness numerically predicted is very close to the one in the hysteresis area of the composite behavior between 12500 and 13500 Nm/rad.

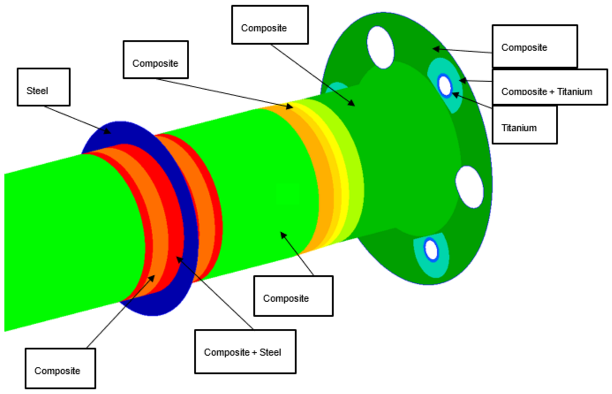

Figure 12: Numerical model of the RECOMPOSE composite shaft

5.4. Dynamic results

The tests carried out have highlighted the main dynamic characteristics of a composite shaft and a line of shafts with two shafts equipped with the interface elements (flectors and bearings). Several key elements should be noted.

5.4.1. Natural frequencies and dominant modes

The impulse tests were carried out on a single shaft in a free-free configuration and then in an articulated-articulated configuration on a bench equipped with flectors and mounted on the ENSAM experimental bearings. The tests identified the early shaft bending modes that are usually the most troublesome during use because they are stressed by residual imbalance and misalignment during rotation. The modes of torsion, tension and compression have not been identified experimentally. Radial or undulating modes may have appeared due to the lack of rigidity in the direction perpendicular to the folds, modes that are very specific to multilayer composites. The tests were compared with finite element calculations (PATRAN/NASTRAN) and an analytical reference model (Euler-Bernoulli beam in bending) having mechanical characteristics E, Young's modulus and rho density such that the first bending frequency corresponds to the first bending mode measured in free-flow.

For these test conditions, out of all the measurements carried out, a first bending mode close to

260 Hz, a second bending mode close to 730 Hz, Figure 13. The axial mode was not observed experimentally, the radial modes were detected by the experiment.

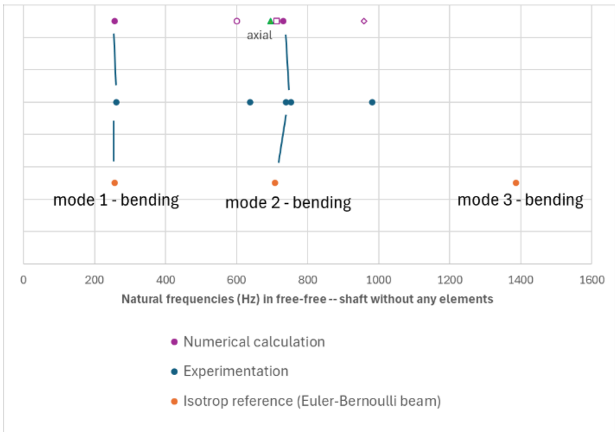

Figure 13: Comparison of natural frequencies between experimentation and modelling; free-free

Using the transfer functions, modal damping was observed on the first mode relatively higher (5-6%) than on the following modes (1-2%). This fairly classic behavior on composite shafts can be explained by several phenomena, often related to the nature of the composites, their manufacture, and the geometry of the shaft. Interlaminar shear or micro-slips between layers can strongly dissipate energy, especially in low-frequency bending deformations (typical of the first mode), and often have lower dissipation at high frequencies.

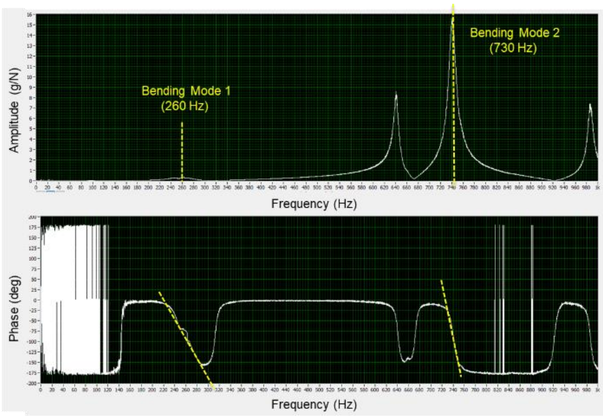

Figure 14: example of free-to-air shock hammer transfer function in L/3

The shock hammer tests on the shaft equipped with flector type coupling elements, as well as with different types of bearings, led to the observation of the impact of boundary conditions on the frequencies (free-free versus articulated-articulated). These tests also led to a comparison with finite element modelling as a function of boundary conditions. The first bending mode is close to 140 Hz and the second mode is close to 520 Hz.

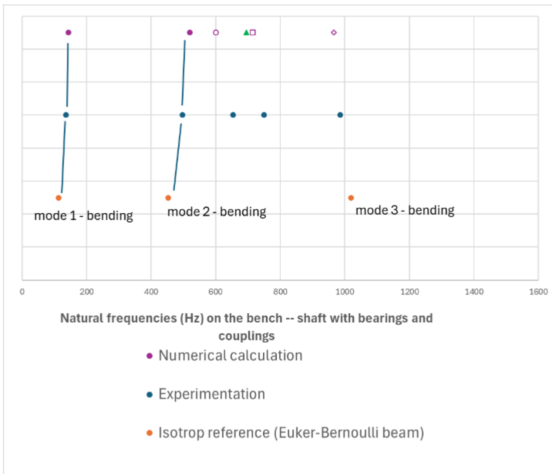

Figure 15: Comparison of natural frequencies between experimentation and modelling; articulated-articulated

These tests showed a relatively expected result consistent with beam theory which leads to the decrease of natural frequencies in the expected proportions, the boundary conditions hardly affecting the radial modes. The analysis of the transfer function revealed the superposition of the frequencies of the shaft and the modes related to the uncoupled bearings. Bearings or flectors do not induce significant additional damping on the first modes. No coupling was observed in the series of two shafts.

5.4.2. *Dynamic response during run-up and constant speed*

The dynamic tests consist of doing the next speed cycle, with 3 speed steps representing the NR (approximately 80 Hz), 80% of the NR and 115% of the NR. The first bending natural frequency being close to 140 Hz, the study and experimental operating regime remains subcritical.

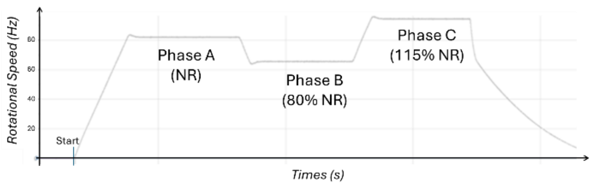

Figure 16: Example of run-up and speed step

The analysis of the vibration levels carried out at constant speed in the different phases, using the measurement of the radial movement of the shaft (laser sensor) or via accelerometers, shows the presence of dominant peaks at the classical rotation frequency (1xW, 2xW and harmonics).

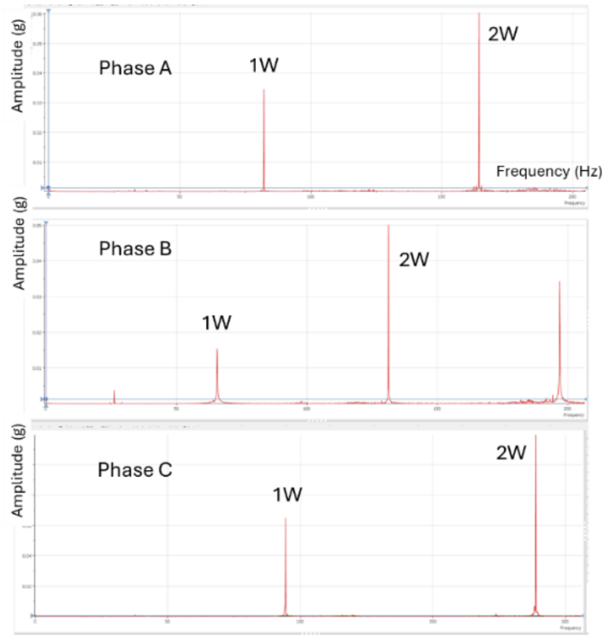

Figure 17: Radial Vibration Amplitude Level at a Point on the Shaft (Laser sensor)

The time-frequency diagrams obtained during the run-up sequences reveal a clear trajectory of the main mode and its harmonics. No instability phenomenon was observed on the explored range, nor the appearance of asynchronous frequencies, nor instability. Measurements made with two shafts in series did not show any coupling between the two shafts.

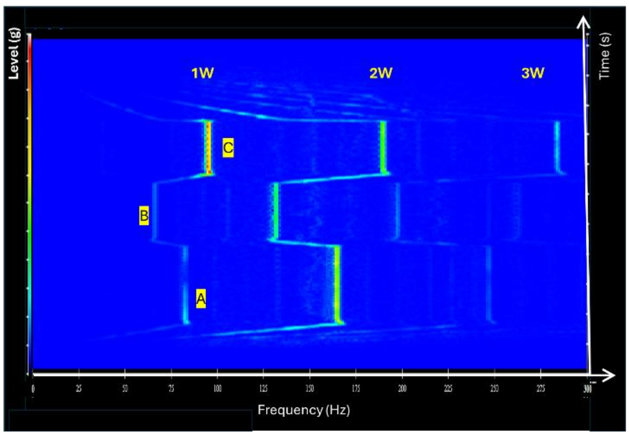

Figure 18: Time-frequency diagram.

5.4.3. Influence of misalignment

The introduction of controlled mechanical misalignments (by lateral play of a few millimeters from 0 to 8 mm) showed little noticeable effect on the vibration response.

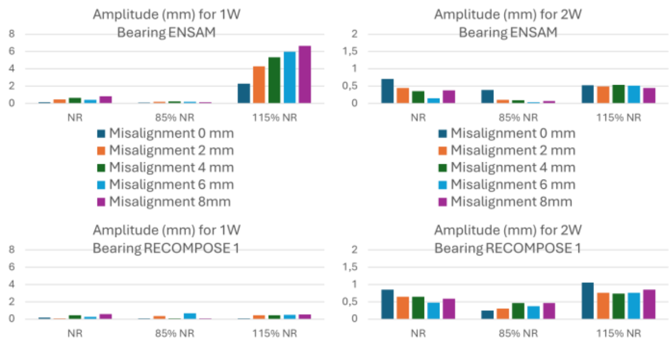

Table 3: 1W and 2W levels depending on misalignment configurations for configuration 2.2

6. CONCLUSIONS AND FUTURE WORK

The test campaign on the one-piece composite drive shafts covered a wide range of aspects required to assess and enhance the technological maturity of this innovative product. Each test performed provided meaningful insights into the shaft's ability to meet the defined specifications.

The stiffness tests formed the basis for evaluating manufacturing process variability and enabled initial correlation with numerical models.

The static tests validated the first specification points by confirming the shaft's resistance to the ultimate torque load. These results also served as baseline data for constructing the shaft's fatigue curve.

The static tests also contributed to a better understanding of the shaft's behavior under multiple loading scenarios, particularly in terms of the various failure patterns observed.

The dynamic Tests of composite transmission shafts involves several key scientific challenges that :

- First challenge: identification of natural frequencies. This step is essential for validating vibration models and anticipating potential resonance risks, particularly in variable-speed regimes.
- Second challenge: characterization of the system's real damping. Damping arises from a complex combination of internal losses (within the composite material — fibers, resin, micro-interfaces) and external mechanical losses (due to interfaces, bearings, and flexible couplings). Accurately quantifying this damping is crucial to assessing the system's long-term dynamic stability.
- Third challenge: superposition of dynamic effects. Measured vibration signals are influenced simultaneously by mass imbalance, potential internal

defects (such as delaminations or inclusions), and assembly effects. Isolating each contribution requires both rigorous methodology and precise instrumentation — which may run counter to the goal of defining a simple, reproducible, and minimalistic experimental protocol.

In this context, the present study validates a simple and efficient experimental approach for investigating the dynamic behavior of composite shaft lines operating in a subcritical regime. The results highlight specific features related to anisotropic structure, mechanical interfaces, and the notable influence of even low-level imbalance.

Preliminary Experimental Observations

A first experimental campaign was conducted on composite drive shafts in a configuration that had not previously been explored. Modal identification using impact hammer testing allowed the determination of the system's natural frequencies. These were found to be in good agreement with predictions from numerical modeling, confirming the validity of the simulation assumptions.

Measured damping ratios were generally low, as expected for this type of structure and material. This low dissipation capacity may become critical under more demanding operating conditions or in the presence of persistent excitations.

Speed ramp-up and ramp-down tests, carried out with clearly defined speed plateaus, did not reveal any abnormal behavior. The vibration spectra showed typical residual components at 1W and 2W (one and two times the rotational speed), with no signs of resonance or nonlinear behavior in the explored subcritical range.

Placing two composite shafts in series did not significantly alter the dynamic response: no additional coupling or vibratory phenomena were observed. Similarly, tests conducted under misalignment conditions — whether radial or angular — did not show any particular sensitivity. Lastly, the influence of flexible couplings (flectors), in terms of relative compliance and damping, was found to have only a marginal effect on the system's global dynamics under the test conditions.

Finally, in addition to the significant progress already achieved on this innovative composite product, further complementary tests are still required. In particular, the fatigue test results should be supplemented with additional tests assessing the static and/or fatigue performance of damaged shafts (BVID – Barely Visible Impact Damage), as well as with environmental testing. These complementary tests will provide insight into the behavior of the shaft and the composite material under degraded conditions and will help verify that the specifications remain fulfilled under such circumstances. Further analysis regarding numerical modelling and failure prediction will be carried out to improve the confidence in numerical models of the single-piece composite drive shaft to design and size this product regarding a given specification.

A. AUTHOR CONTACT

BARLET-BAS Sébastien, sebastien.barlet-bas@nexteam-group.com

MALBURET François, francois.malburet@ensam.eu

LOPEZ Cédric, cedric.lopez@nexteam-group.com

PIERREL Bruno, bruno.pierrel@nexteam-group.com

B. ACKNOWLEDGMENTS

This project is funded by the European Union NextGeneration EU, the DGAC and is supported by CORAC, it aims to increase the competitiveness of helicopters while reducing their CO2 emissions.

C. REFERENCES

1. Bilalis, E., Keramidis and M., Tsouvalis, N., "Structural design optimization of composite materials drive shafts", Marine Structures, Vol. 84, 2022, 103194, https://doi.org/10.1016/j.marstruc.2022.103194
2. Qi, L., Li, C., Yu, X., Min, W., Shi, H., Tao, L., Wang, H., Yu, M., Ni, L. and Sun, Z., "Effect of reinforced fibers on the vibration characteristics of fibers reinforced composite shaft tubes with metal flanges", Composite Structures, Vol. 275, 2021, 114460, https://doi.org/10.1016/j.compstruct.2021.114460

3. Barlet-Bas S., Malburet F., Lopez C. and Pierrel, B., “Development of a weight-optimized single-piece composite drive shaft for tail drive line application”, 50th European Rotorcraft Forum, 2024, Marseille, France, September
4. Kamboh MS., Machhi M.A., Kamboh M.F., Jayanaidu P. and Hibbatullah M., “Design and Analysis of Drive Shaft with a Critical Review of Advance Composite Materials and the Root Causes of Shaft Failure”, International Research Journal of Engineering and Technology (IRJET), 2020, Vol. 7, (06):12.
5. Gupta K., “Composite Shaft Rotor Dynamics: An Overview”, Vibration Engineering and Technology of Machinery, edited by J.K. Sinha, Mechanisms and Machine Science, Vol 23, Springer International Publishing; 2015:79-94. doi:10.1007/978-3-319-09918-7_6
6. Palumbo, D. and De Finis, R., “Fatigue and Fracture Behavior of Composite Materials”. Materials, 2023, Vol. 16, 7292, https://doi.org/10.3390/ma16237292
7. Gao, J.X., Fei H., Yi-Ping Y., and Yuan-Yuan L., 2023. “Fatigue Reliability Analysis of Composite Material Considering the Growth of Effective Stress and Critical Stiffness”, Aerospace, 2023, Vol. 10, (9): 785. https://doi.org/10.3390/aerospace10090785
8. Montagnier, O., and Hochard. C., “Dynamics of a Supercritical Composite Shaft Mounted on Viscoelastic Supports”, Journal of Sound and Vibration, Vol. 333, (2), 2014, pp. 470-484. https://doi.org/10.1016/j.jsv.2013.09.021.
9. Jacquet-Richardet G., Chatelet E. and Nouri-Baranger T., “Rotating Internal Damping in the Case of Composite Shafts”, edited by IUTAM Symposium on Emerging Trends in Rotor Dynamics. Vol 1011. IUTAM Bookseries. Springer Netherlands; 2011:125-134. doi:10.1007/978-94-007-0020-8_11
10. Sino, R., Nouri Baranger, T., Chatelet, E., and Jacquet G., “Dynamic Analysis of a Rotating Composite Shaft”, Composites Science and Technology, Vol. 68, 2008, 337-345, http://dx.doi.org/10.1016/j.compscitech.2007.06.019
11. "The composite materials handbook (MIL handbook 17). Volume 3: Materials usage, design, and analysis.", Jan. 1999, section 9.2.3

D. CLASSIFICATION & COPYRIGHT